VIII International Conference on Particle-Based Methods
PARTICLES 2023
U. Perego, M. Cremonesi, A. Franci (Eds)

COMPARISON OF INCOMPRESSIBLE AND WEAKLY-COMPRESSIBLE SPH FOR THE SIMULATION OF LASER BEAM WELDING

Daniel Sollich and Peter Eberhard

Institute of Engineering and Computational Mechanics
University of Stuttgart
Pfaffenwaldring 9, 70569 Stuttgart, Germany
{daniel.sollich, peter.eberhard}@itm.uni-stuttgart.de, www.itm.uni-stuttgart.de/en

Abstract: The process of laser beam welding is simulated using the Weakly-Compressible Smoothed Particle Hydrodynamics (WCSPH) and the Incompressible SPH (ISPH) methods. The presented models consider significant physical effects such as heat conduction, temperature-dependent surface tension with wetting, the phase transitions melting and solidification, and an evaporation-induced recoil pressure. Here, particular emphasis is placed on the modeling differences between the WCSPH and ISPH methods. Then, both methods are evaluated in terms of their accuracy and performance in the simulation of deep penetration laser beam welding with oscillating laser power.

Keywords. Laser Beam Welding, SPH, Laser Power Modulation, Capillary Depth

1 INTRODUCTION

Laser beam welding is a joining technique that is gaining popularity due to its high welding speed, low thermal distortion, and ease of automation. However, the process becomes easily unstable and weld defects such as pores or spatter can occur that reduce the weld seam strength. To better understand all the physical effects leading to the weld defects, numerical simulations are often used as experimental observations are limited due to inaccessibility. The simulation of the laser beam welding process is demanding due to the rapidly changing interfaces between the solid metal, liquid melt, and vapor. In contrast to mesh-based methods, the Smoothed Particle Hydrodynamics (SPH) method is able to intrinsically capture the complex interface due its mesh-free nature. The SPH method can be divided into the Weakly-Compressible SPH (WCSPH) and the Incompressible SPH (ISPH) method. In the current state of the art, both methods demonstrate promising results in the application to laser material processing as shown in [1, 2, 3].

In this work, the laser beam welding model in [4] based on the WCSPH method is extended to be simulated with ISPH. The presented models are applied to deep penetration laser beam welding with sinusoidal laser power oscillation. The aim of this work is to examine the modeling differences between the WCSPH and ISPH methods, as well as their accuracy and performance for the simulation of laser beam welding. Furthermore, the influence of an oscillating laser power on the laser welding process is investigated for the first time with the SPH method.

2 MODELING APPROACH

The modeling of laser beam welding requires the consideration of the laser-material interaction, and the fluid and thermodynamics. The laser-material interaction is modeled by coupling the SPH method with a ray tracer as described in [5]. Based on the laws of geometrical optics, the ray tracer calculates the spatially absorbed intensity distribution on the capillary surface by taking into account multiple reflections of the laser beam within the capillary. The fluid and thermodynamics is modeled using the SPH method as described in the following. First, the SPH model for laser beam welding based on the approach in [4] is briefly presented. Next, the modeling differences between WCSPH and ISPH for the simulation of laser beam welding are outlined.

2.1 SPH Model

The SPH method is a mesh-free Lagrangian particle method commonly used in hydrodynamics. In the SPH method, the fluid is described by a set of freely moving interpolation points, so-called particles. To determine the fluid movement, the incompressible Navier-Stokes equations are applied and represented by a sum over neighboring particles using a smoothing kernel function. The main advantage of the SPH method is its Lagrangian and mesh-free nature, which allows to describe arbitrary and rapidly changing interfaces and free surfaces.

For laser beam welding, the SPH equations guaranteeing the kinematics, conservation of mass, momentum (incompressible Navier-Stokes equation), and energy are given by

$$\frac{\mathrm{d}\boldsymbol{r_a}}{\mathrm{d}t} = \boldsymbol{v}_a \,, \tag{1}$$

$$\frac{\mathrm{d}\rho_a}{\mathrm{d}t} = \rho_a \sum_b \frac{m_b}{\rho_b} \left(\boldsymbol{v}_a - \boldsymbol{v}_b\right) \cdot \nabla_a W_{ab} \,, \tag{2}$$

$$\frac{\mathrm{d}\boldsymbol{v}_a}{\mathrm{d}t} = -\sum_b m_b \frac{p_a + p_b}{\rho_a \rho_b} \nabla_a W_{ab} + \left\{ \frac{\mu}{\rho} \nabla^2 \boldsymbol{v} \right\}_a + \boldsymbol{a}_{\mathrm{g},a} + \boldsymbol{a}_{\mathrm{s},a} \,, \tag{3}$$

$$\frac{\mathrm{d}T_a}{\mathrm{d}t} = \frac{1}{\rho_a c_\mathrm{p}} \left(\left\{ \lambda \nabla^2 T \right\}_a + \dot{q}_{\mathrm{s},a} + \dot{q}_{\mathrm{r},a} \right) \,, \tag{4}$$

where t is the time, $\boldsymbol{r}$ the position, ρ the density, $\boldsymbol{v}$ the velocity, m the mass, W the smoothing kernel function, p the pressure, μ the dynamic viscosity, $\boldsymbol{a}_\mathrm{g}$ and $\boldsymbol{a}_\mathrm{s}$ the accelerations due to gravitational and surface forces, T is the temperature, c_p the heat capacity, and λ the heat conductivity. The surface forces are modeled using the Continuum Surface Force (CSF) method and include the temperature-dependent surface tension with wetting and the evaporation-induced recoil pressure. Furthermore, the terms $\mu \nabla^2 \boldsymbol{v} / \rho$ describe the viscous force, $\lambda \nabla^2 T$ the heat transfer by heat conduction, $\dot{q}_\mathrm{s}$ the absorbed heat of the laser beam, and $\dot{q}_\mathrm{r}$ the heat losses of the evaporated material.

2.2 Comparison of the WCSPH and ISPH Model

In the following, the modeling differences between ISPH and WCSPH for the simulation of laser beam welding are presented.

2.2.1 Pressure Calculation

The fundamental differences between the WCSPH and ISPH methods are the treatment of density and the calculation of pressure in Eq. (3). In the WCSPH method, small density changes are allowed, and the pressure is related to the density by an artificial equation of state [6]. In this work a simplified equation of state is used

$$p_a = c_0^2 \left(\rho_a - \rho_0\right) , \tag{5}$$

where c_0 is the numerical speed of sound, and ρ_0 the reference density. The WCSPH approach is simple to implement and parallelize. However, the WCSPH method requires additional numerical improvements, which are described in the next section.

In the ISPH method, the density is kept constant by enforcing the incompressibility condition $\nabla \cdot \boldsymbol{v} = 0$. To relate the unknown pressure to the velocity, the projection method is applied that projects an intermediate velocity field $\boldsymbol{v}^*$ onto a divergence-free space [7]. The pressure is then obtained by solving the pressure Poisson equation

$$\nabla \cdot \left(\frac{1}{\rho} \nabla p^{t+\Delta t} \right) = \frac{1}{\Delta t} \nabla \cdot \boldsymbol{v}^* . \tag{6}$$

In contrast to the fully explicit WCSPH method, the ISPH method is semi-implicit. The pressure is solved implicitly, while the velocity is calculated explicitly. Due to the implicit solution procedure, the ISPH method requires additional effort to solve the pressure-Poisson equation, but also allows larger time step sizes compared to the WCSPH method.

2.2.2 Numerical Stability

In its standard formulation, the WCSPH method suffers from spurious numerical oscillations in the density field and particle clumping. To overcome these problems, correction techniques such as artificial viscosity [8], artificial stress [9], and δ-SPH [10] are applied.

In contrast, the ISPH method does not require any of the above correction techniques. Typically, only the particle shifting technique is applied to ensure a uniform particle distribution by shifting the particles slightly away from the streamlines [11]. However, in the simulation of laser beam welding, spurious interface flows are observed. These interface flows are a well-known problem of the CSF method which is used here for the calculation of the surface forces. Since the physical viscosity is not sufficient to damp the interface flows caused by numerical effects, an increased numerical viscosity is applied at the solid-liquid interface and at the free surface as suggested in [12].

2.2.3 Thermal Expansion and Convection

In the WCSPH method, volumetric thermal expansion is modeled according to [13] by simply introducing a temperature-dependent reference density into the equation of state in Eq. (5) as

$$p_a = c_0^2 \left(\rho_a - \rho_0 \left(T_a\right)\right) . \tag{7}$$

Since the pressure is now related to the temperature, the particles change their 'volume' depending on the temperature. In addition, the formulation accounts also for convection caused by density variations due to temperature.

In the ISPH method, thermal expansion is not considered because the density is constant there. However, thermal convection is taken into account by the temperature-dependent buoyancy using the Boussinesq approximation as proposed in [3]

$$\boldsymbol{a}_{\mathrm{g}} \left(T_a\right) = \boldsymbol{g} \left(1 - \beta \left[T_a - T_0\right]\right) , \tag{8}$$

where $\boldsymbol{g}$ is the gravitational acceleration, β the thermal expansion coefficient, and T_0 the reference temperature. Note that the Boussinesq approximation can also be applied in the WCSPH regime instead of the previously mentioned approach.

2.2.4 Thermoelastic Material Behavior

The SPH method can be used not only to solve hydrodynamic problems, but also to simulate the elastic deformation of solid bodies [6]. To model elastic material behavior, the pressure in Eq. (3) is replaced by the Cauchy stress tensor

$$\sigma_a^{ij} = -p_a \delta^{ij} + S_a^{ij} , \tag{9}$$

where δ^{ij} is the Kronecker delta, and S^{ij} the deviatoric stress tensor. Since the same equation of state in Eq. (7) can be used for the pressure evaluation in Eq. (9), the extension of the WCSPH model to elastic material behavior is rather simple. For this reason, thermoelastic material behavior is additionally considered in the WCSPH model. In contrast, the solid phase is modeled using fixed fluid particles with zero velocity and acceleration in the ISPH model. Once the melting temperature is reached, the velocity and acceleration of the particles are calculated.

Table 1: Model variations used in this work

	numerical viscosity	thermal expansion and convection	solid phase
WCSPH	artificial [8]	thermal expansion [13]	elastic [6]
WCSPH red.	artificial [8]	Boussinesq approx. [3]	fixed
WCSPH red., int. visc.	interface [12]	Boussinesq approx. [3]	fixed
ISPH	interface [12]	Boussinesq approx. [3]	fixed

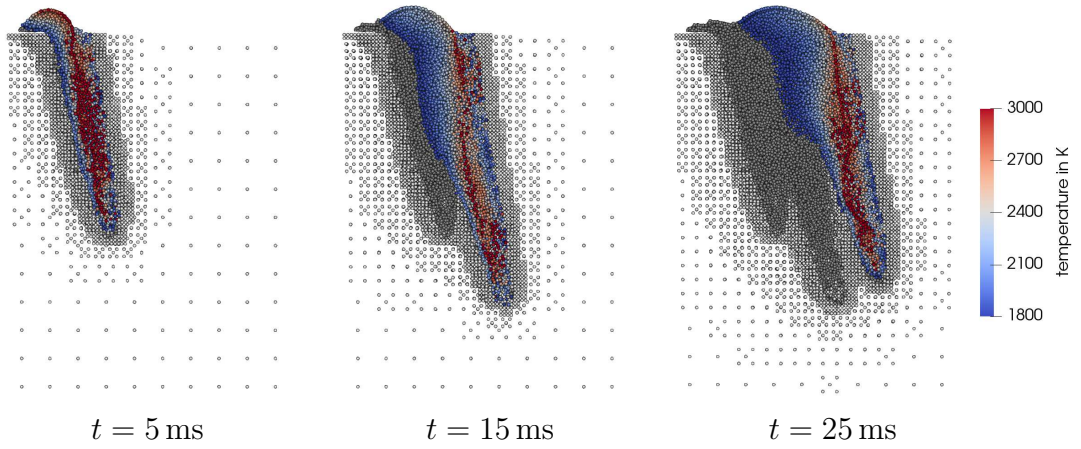

(a) WCSPH

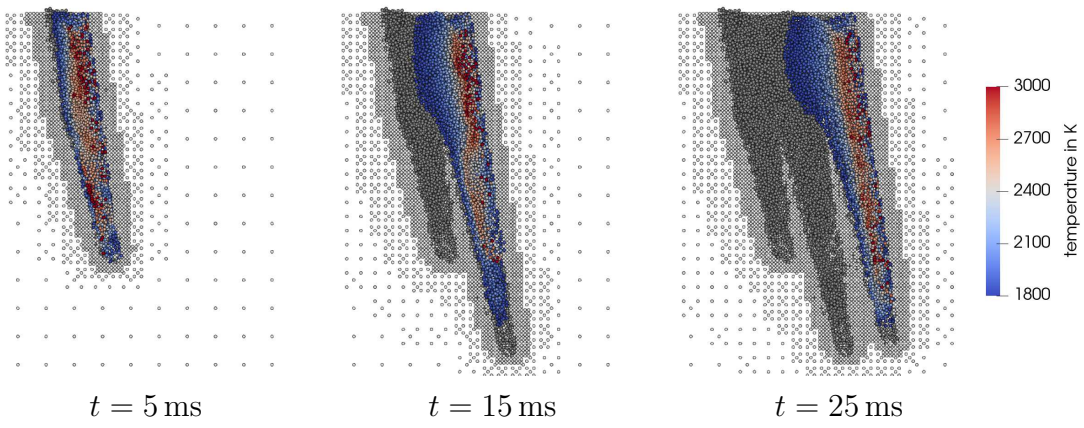

(b) ISPH

Figure 1: Deep penetration laser beam welding of iron with sinusoidal laser power oscillation at frequency $f = 100\,\mathrm{Hz}$, an average laser power of 2.25 kW and an amplitude of 1.75 kW. The temperature distribution is shown for liquid particles, and re-solidified particles are highlighted in dark-gray.

3 SIMULATION RESULTS

In the following, deep penetration laser beam welding of iron and aluminum is simulated. The process parameters are chosen according to the experiments in [14]. The laser beam has a focal diameter of 0.2 mm, an angle of incidence of 10 °, and is moved along the x-axis at a constant feed rate of 4 m/min. Further, the laser power is oscillating with an average laser power of 2.25 kW and an amplitude of 1.75 kW for iron and an average laser power of 2.5 kW and an amplitude of 1.5 kW for aluminum. The iron workpiece has dimensions $4.0 \times 2.4 \times 6.0\,\mathrm{mm}^3$, while the aluminum workpiece has dimensions $7.2 \times 4.0 \times 5.2\,\mathrm{mm}^3$. During the simulation, dynamic particle refinement according to [15] with three refinement levels is applied, resulting in a particle spacing of 0.05 mm for the finest resolution level. In order to analyze the effect of the modeling differences be-

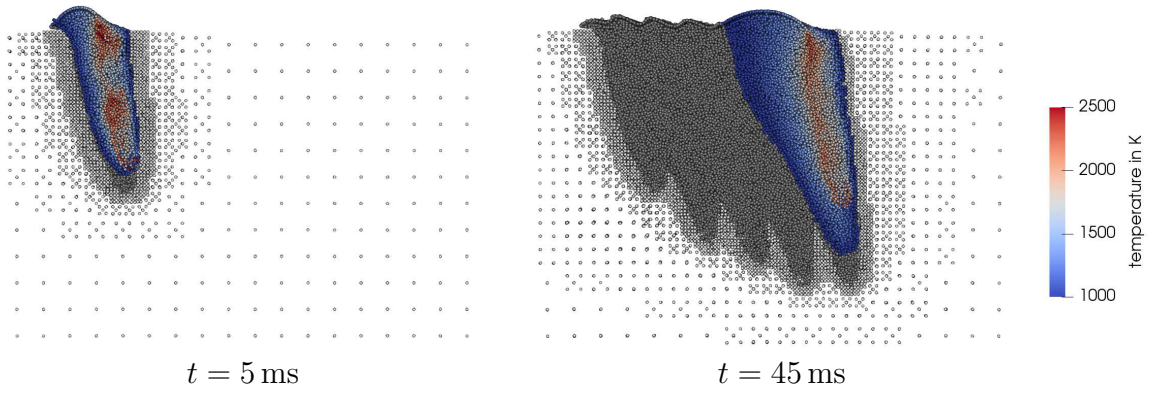

(a) WCSPH

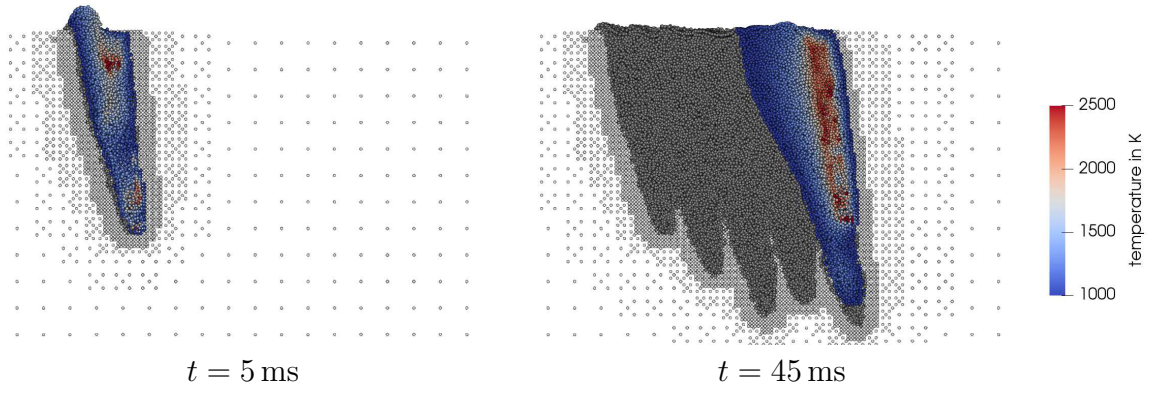

(b) ISPH

Figure 2: Deep penetration laser beam welding of aluminum with sinusoidal laser power oscillation at frequency $f = 100\,\mathrm{Hz}$, an average laser power of $2.5\,\mathrm{kW}$ and an amplitude of $1.5\,\mathrm{kW}$. The temperature distribution is shown for liquid particles, and re-solidified particles are highlighted in dark-gray.

tween the ISPH and WCSPH methods described in Section 2.2, different model variations are simulated. An overview of the variations is given in Tab. 1.

The simulated laser welding process is shown for a laser power frequency $f = 100\,\mathrm{Hz}$ in Fig. 1 for iron and in Fig. 2 for aluminum. In the simulation, a capillary is formed within the liquid melt pool. The low frequency of the laser power oscillation results in a non-constant depth of the re-solidified weld seam. Comparing the WCSPH and ISPH simulations, the size of the liquid melt pool and of the re-solidified weld seam are in good agreement. Due to the volumetric thermal expansion of the material in WCSPH, melt protrusions at the surface are observed.

In the following, the capillary depth is plotted over time in Fig. 3 to investigate the response of the capillary to the laser power signal. It can be observed, that the capillary depth is oscillating due to the sinusoidal laser power signal, with the depth increasing at high laser power and decreasing at low laser power. In addition, the oscillation of the capillary depth is delayed compared to the laser power signal, which means that the capillary requires additional time to follow the laser power signal.

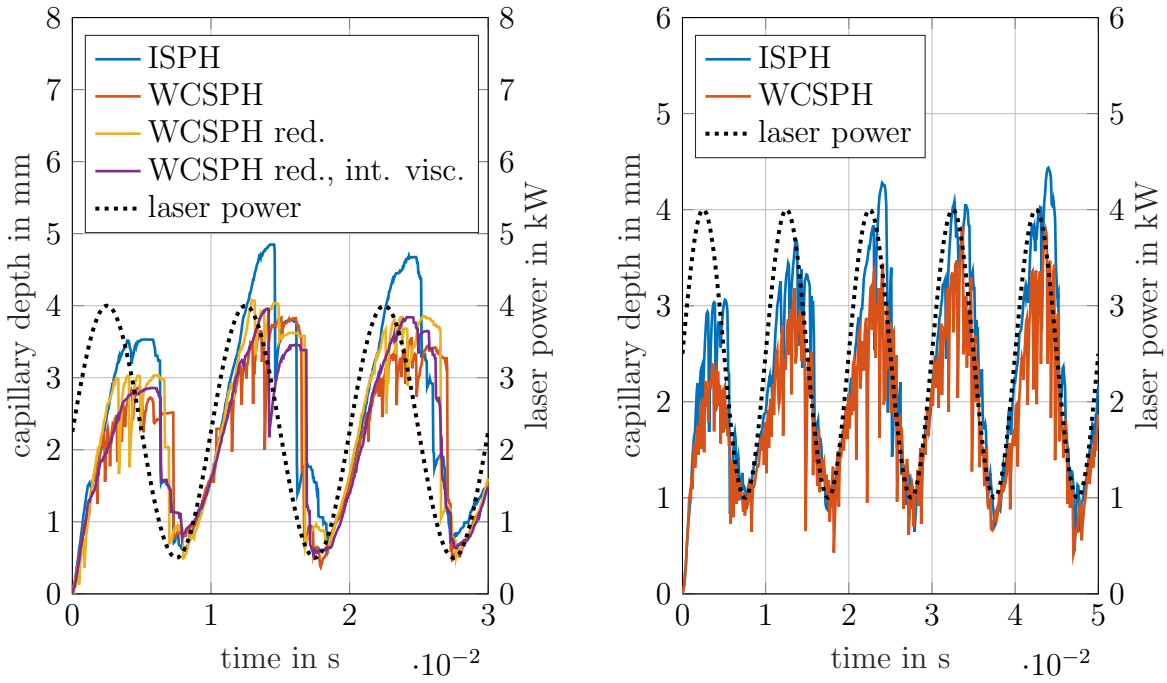

(a) iron (b) aluminum

Figure 3: Capillary depth for sinusoidal laser power oscillation at frequency $f = 100\,\mathrm{Hz}$.

Comparing WCSPH and ISPH, the curves of the capillary depth agree well. However, the maximum capillary depth is larger in the ISPH simulation. To limit the possible causes of the deeper capillary in the ISPH simulation, the WCSPH model is modified so that it differs only in the pressure calculation and correction techniques, see Tab. 1. Since a deeper capillary is obtained in ISPH despite the same modeling approach for the physical effects and numerical viscosity, these effects can be excluded as a possible cause.

For WCSPH, the different model variations in Fig. 3(a) have hardly any influence on the capillary depth. In particular, the maximum depth decreases slightly when thermal expansion is taken into account. The cause for this effect may be the increase in fluid volume. Furthermore, the use of artificial or interfacial viscosity has little effect on the maximum capillary depth. However, the interfacial viscosity smoothes out oscillations in the capillary depth. The reason for this is that high surface tension forces, which normally cause the capillary to collapse, are dampened by equally high viscous forces of the interface viscosity.

Regarding the computational efficiency, the ISPH simulation is faster. The larger time step size (2.7 times for iron and 3.9 times for aluminum) outweighs the additional effort of the implicit solution procedure. For the simulations in iron, the ISPH method is 2.4 times faster than the WCSPH model with thermoelastic material behavior, and 2.0 times faster than the WCSPH model without thermoelasticity. For aluminum, the speedup is 3.7 . The simulations were carried out in parallel using 6 cores on a desktop PC with an AMD Ryzen™ Threadripper™ 3960X CPU.

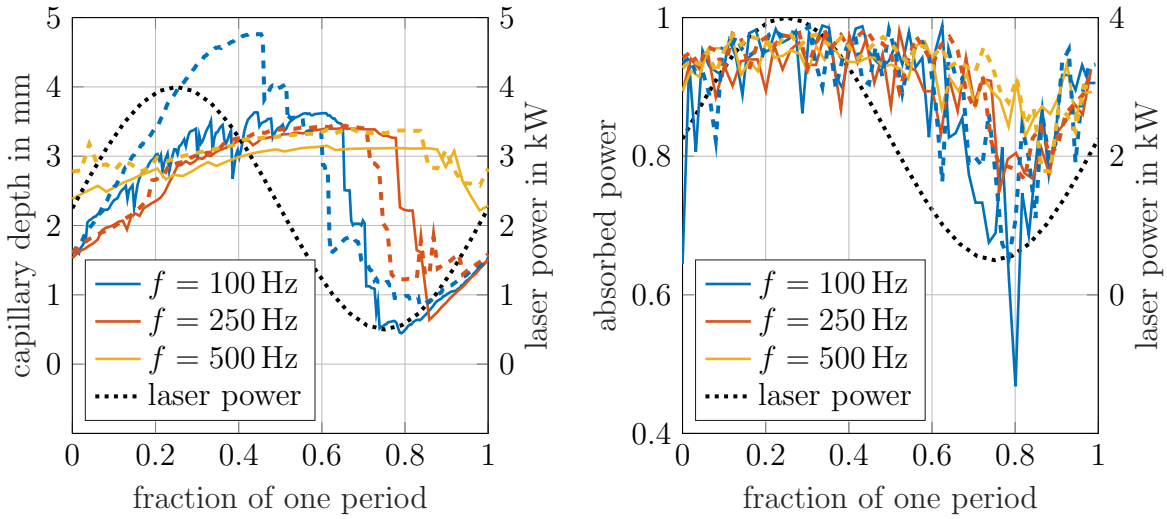

(a) capillary depth

(b) absorbed laser beam power

Figure 4: Quasi-stationary periodic behavior of the capillary depth and absorbed power for deep penetration laser beam welding of iron with sinusoidal laser power oscillation. The solid lines (——) represent the WCSPH method, while the dashed lines (- - -) are simulated using the ISPH method.

In the following, another physical investigation is performed, i.e. the influence of the oscillation frequency of the laser power is analyzed. In Fig. 4 the capillary depth and the absorbed laser power are averaged over all periods in the quasi-stationary state for the oscillation frequencies $f = 100$, 250 and 500 Hz. The results show that the capillary depth and absorbed laser power are also oscillating for all frequencies applied. With increasing frequency, the amplitude of the oscillating capillary depth and absorbed laser power decreases. Furthermore, the increase and abrupt decrease of the depth is increasingly delayed for higher frequencies. The abrupt decrease in capillary depth can be explained by the decreasing laser power towards the end of each oscillation, and by the decrease in the fraction of absorbed laser power once the capillary has collapsed.

Next, the simulation results are compared to experimental measurements in [14] in order to evaluate the accuracy of the WCSPH and ISPH simulations. In Fig. 5, the amplitude ratio between the capillary depth and laser power oscillation is plotted. This value is taken as an estimate for the ability of the capillary to change its depth in dependence of the laser power. For low oscillation frequencies $f = 100$ and 250 Hz, the change rate of capillary depth per laser power are in a similar range for iron and aluminum. For high oscillation frequencies $f = 500$ Hz, the capillary depth is less capable to follow the laser power for iron compared to aluminum. This result is independent of the applied method, and agrees well with the experimental observations. However, the simulated values are significantly larger than in the experiment. The reason for this may be the different approaches for determining the capillary depth between simulation and experiment, inaccuracies in the simulation models, or in the experimental measurements, or all of these together.

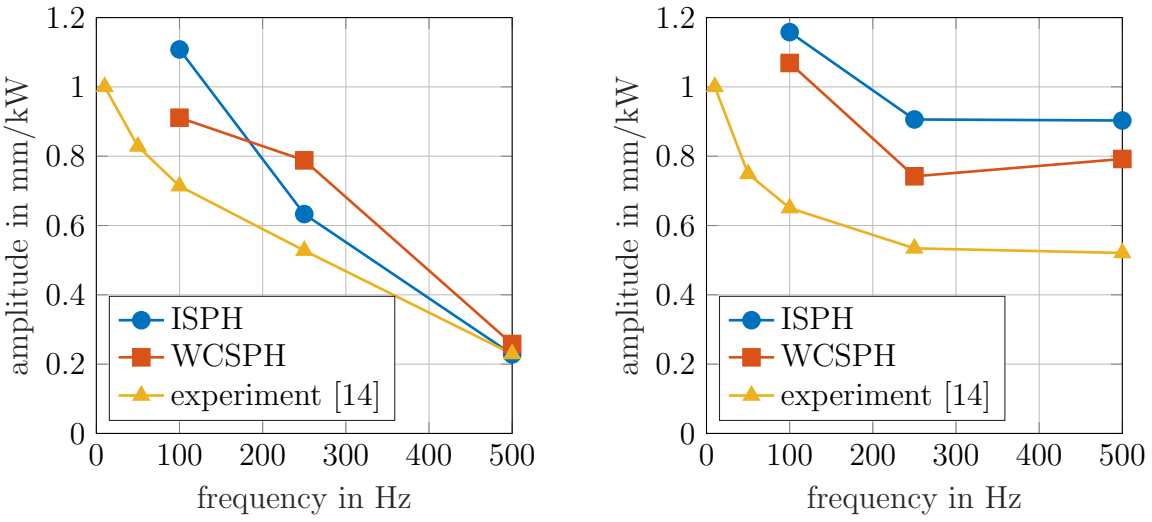

(a) iron

(b) aluminum

Figure 5: Amplitude ratio between the capillary depth and laser power oscillation for deep penetration laser beam welding with sinusoidal laser power oscillation.

4 CONCLUSIONS

In this contribution, laser beam welding with an oscillating laser power is simulated using the WCSPH and ISPH methods. The aim is to evaluate both methods in terms of modeling capability, accuracy, and performance.

Regarding the modeling approach, the methods differ in the calculation of the pressure, as well as in the method-specific approaches to increase numerical stability. While most of the physical effects are modeled identically, the WCSPH method is numerically advantageous in the modeling of thermal expansion and convection. In addition, the thermoelastic material behavior is considered here in the WCSPH model due to the similar structure of the algorithm. In the simulation, both models are able to represent the main characteristics of the laser beam welding process as the formation of a capillary. The comparison of the simulation results with experimental measurements shows good agreement in the response of the resulting capillary depth to the oscillating laser power signal. With both methods, the depths are overestimated, whereby the WCSPH method is slightly closer to the experimental results. In terms of computational efficiency, the ISPH simulation is faster. Here, the larger possible time step size of the ISPH method outweighs the additional effort of the implicit solution method.

ACKNOWLEDGMENT

The research leading to the presented results was funded by the Deutsche Forschungsgemeinschaft (DFG, German Research Foundation) in projects 266218804, 405605200, and 439917965. This support is highly appreciated.

REFERENCES

[1] Afrasiabi, M.; Keller, D.; Lüthi, C.; Bambach, M.; Wegener, K.: Effect of Process Parameters on Melt Pool Geometry in Laser Powder Bed Fusion of Metals: a Numerical Investigation. Procedia CIRP, Vol. 113, pp. 378–384, 2022.

[2] Bierwisch, C.; Dietemann, B.; Najuch, T.: Accurate Laser Powder Bed Fusion Modelling Using ISPH. In Proceedings of the 17th International Smoothed Particle Hydrodynamics European Research Interest Community Workshop (SPHERIC 2023), Rhodes, Greece, pp. 255–261, 2023.

[3] Fürstenau, J.P.; Weißenfels, C.; Wriggers, P.: Incompressible Simulation of the Selective Laser Melting Process. In Proceedings of the 15th International Smoothed Particle Hydrodynamics European Research Interest Community Workshop (SPHERIC 2021), Newark, NJ, USA, pp. 395–402, 2021.

[4] Sollich, D.; Reinheimer, E.N.; Wagner, J.; Berger, P.; Eberhard, P.: An Improved Recoil Pressure Boundary Condition for the Simulation of Deep Penetration Laser Beam Welding Using the SPH Method. European Journal of Mechanics - B/Fluids, Vol. 96, pp. 26–38, 2022.

[5] Hu, H.; Fetzer, F.; Berger, P.; Eberhard, P.: Simulation of Laser Welding Using Advanced Particle Methods. GAMM-Mitteilungen, Vol. 39, No. 2, pp. 149–169, 2016.

[6] Monaghan, J.J.: Smoothed Particle Hydrodynamics and Its Diverse Applications. Annual Review of Fluid Mechanics, Vol. 44, pp. 323–346, 2012.

[7] Cummins, S.J.; Rudman, M.: An SPH Projection Method. Journal of Computational Physics, Vol. 152, No. 2, pp. 584–607, 1999.

[8] Monaghan, J.J.; Gingold, R.A.: Shock Simulation by the Particle Method SPH. Journal of Computational Physics, Vol. 52, No. 2, pp. 374–389, 1983.

[9] Monaghan, J.J.: SPH Without a Tensile Instability. Journal of Computational Physics, Vol. 159, No. 2, pp. 290–311, 2000.

[10] Antuono, M.; Colagrossi, A.; Marrone, S.; Molteni, D.: Free-Surface Flows Solved by Means of SPH Schemes with Numerical Diffusive Terms. Computer Physics Communications, Vol. 181, No. 3, pp. 532–549, 2010.

[11] Lind, S.J.; Xu, R.; Stansby, P.K.; Rogers, B.D.: Incompressible Smoothed Particle Hydrodynamics for Free-Surface Flows: A Generalised Diffusion-Based Algorithm for Stability and Validations for Impulsive Flows and Propagating Waves. Journal of Computational Physics, Vol. 231, No. 4, pp. 1499–1523, 2012.

[12] Meier, C.; Fuchs, S.L.; Hart, A.J.; Wall, W.A.: A Novel Smoothed Particle Hydrodynamics Formulation for Thermo-Capillary Phase Change Problems with Focus on Metal Additive Manufacturing Melt Pool Modeling. Computer Methods in Applied Mechanics and Engineering, Vol. 381, p. 113812, 2021.

[13] Russell, M.; Souto-Iglesias, A.; Zohdi, T.: Numerical Simulation of Laser Fusion Additive Manufacturing Processes Using the SPH Method. Computer Methods in Applied Mechanics and Engineering, Vol. 341, pp. 163–187, 2018.

[14] Fetzer, F.; Boley, M.; Weber, R.; Graf, T.: Comprehensive Analysis of the Capillary Depth in Deep Penetration Laser Welding. In High-Power Laser Materials Processing: Applications, Diagnostics, and Systems VI, Vol. 10097, pp. 73–80, SPIE, 2017.

[15] Sollich, D.; Eberhard, P.: Adaptive Smoothed Particle Hydrodynamics for the Simulation of Laser Beam Welding Processes. In Proceedings of the 15th International Smoothed Particle Hydrodynamics European Research Interest Community Workshop (SPHERIC 2021), Newark, NJ, USA, pp. 158–165, 2021.